Refrigeration below 1K

1. Dilution refrigerator
2. Adiabatic demagnetization
3. Pomeranchuk cooling

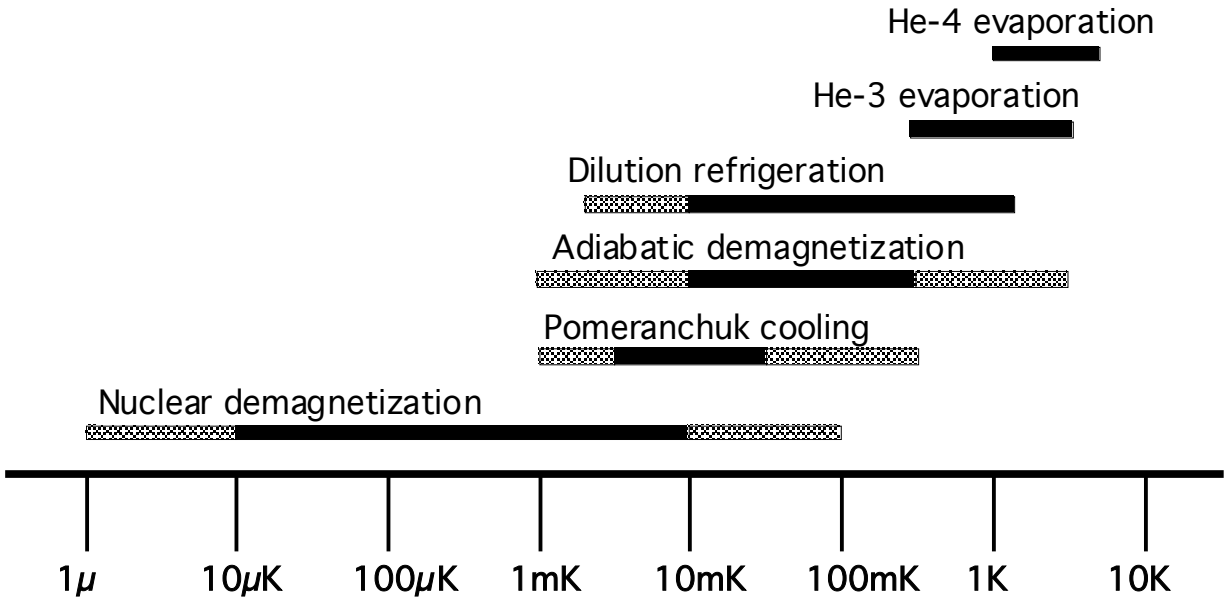

Dilution refrigerators

The phase diagram of $^3He/^4He$

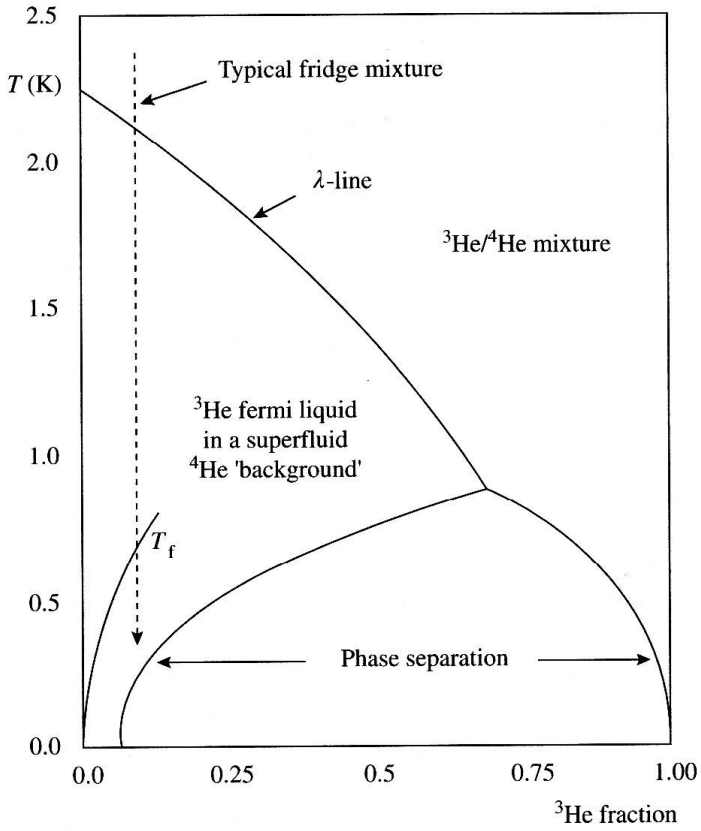

FIG. 8.3 The schematic phase diagram of liquid helium mixtures.

Phase separation occurs somewhere below 0.8K depending on the mixture

Note that the He^4-rich phase contains 6.6% He^3 even at T=0

Where does the He^3 atom want to be.

Chemical potential for He-3 in different environments.

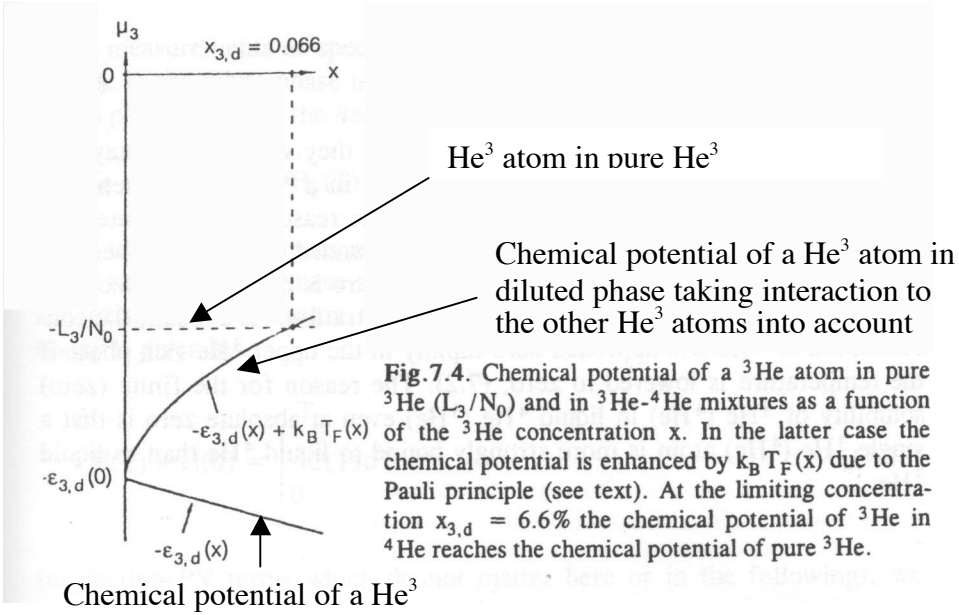

Fig.7.4. Chemical potential of a ^3He atom in pure ^3He (L_3/N_0) and in ^3He-^4He mixtures as a function of the ^3He concentration x. In the latter case the chemical potential is enhanced by $k_B T_F(x)$ due to the Pauli principle (see text). At the limiting concentration $x_{3,d}$ = 6.6% the chemical potential of ^3He in ^4He reaches the chemical potential of pure ^3He.

Chemical potential of a He^3 atom in diluted phase

Binding energy is smaller in He^4 due to lower mass, giving larger zero point fluctuations.

He^3 in He^4 can be treated as a dilute Fermi liquid. The superfluid helium 4 acts as an inert background.

$m^* \approx 2.34\text{-}2.8\ m_3$, $T_{F,conc} \approx 1K$

$T_{F,dil} \sim x^{2/3}$

Schematic drawing of a dilution refrigerator

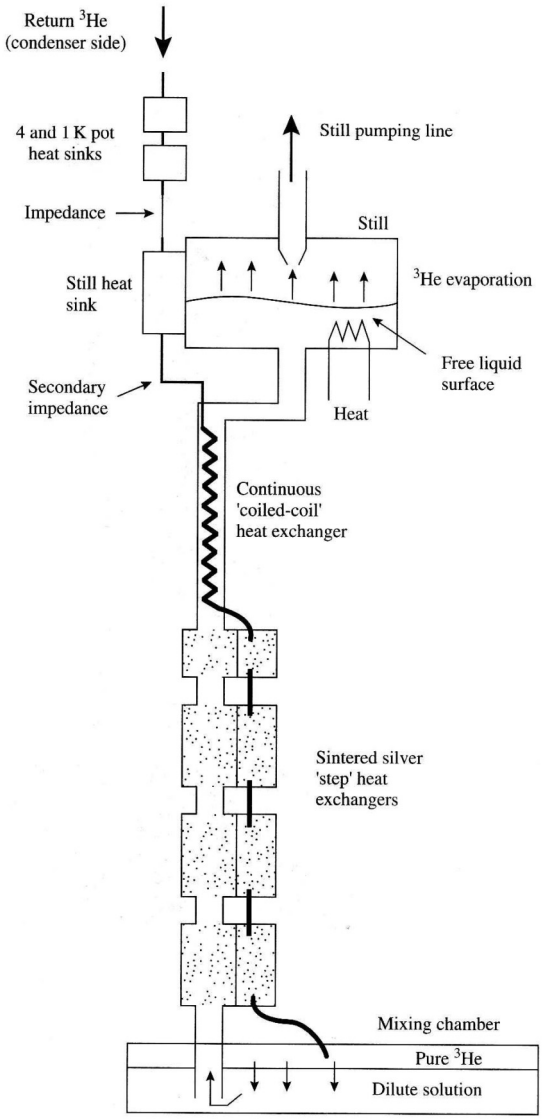

FIG. 8.1 A dilution refrigerator in schematic form.

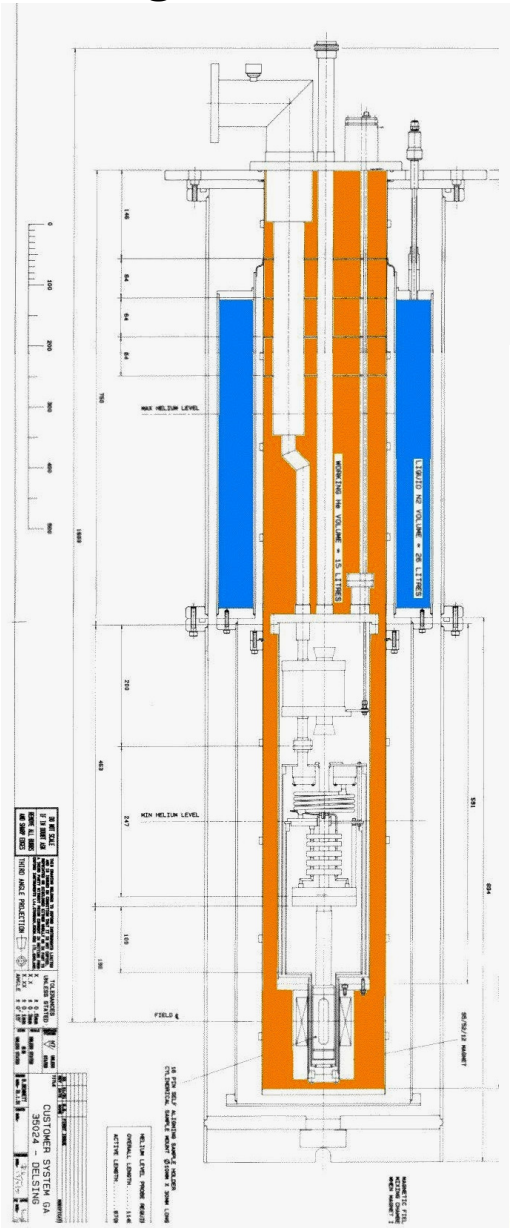

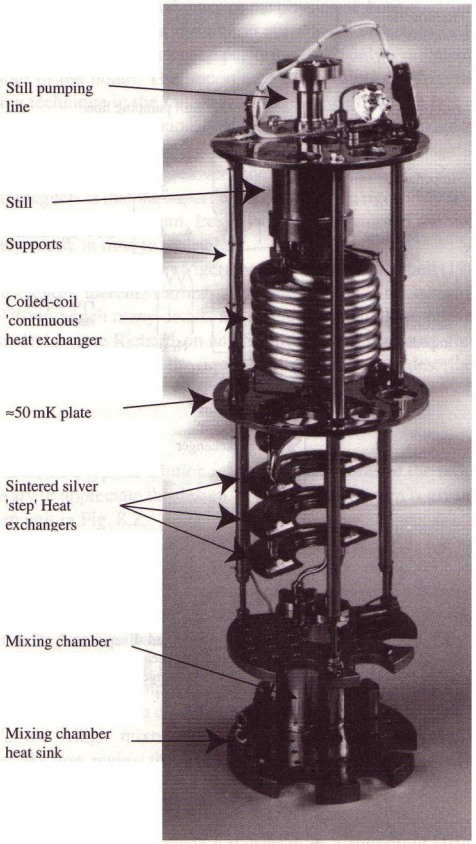

FIG. 8.2 A modern dilution refrigerator. Courtesy of Oxford Instruments.

Cooling power for a dilution refrigerator

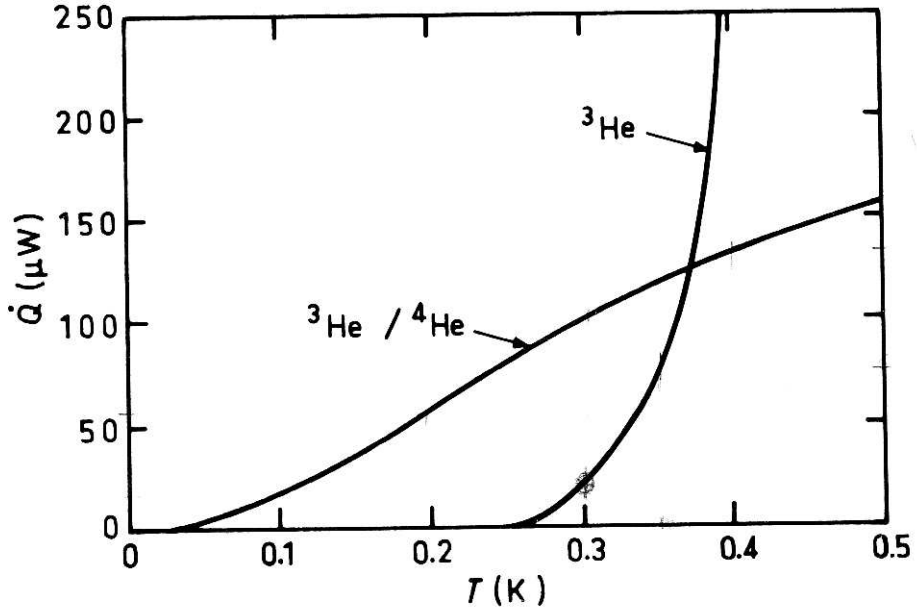

Fig. 3.7. The cooling powers of a ^{3}He evaporation cryostat and of a ^{3}He/^{4}He dilution refrigerator as functions of temperature. It has been assumed that the pump used can handle 5 liter/sec of gas at all relevant pressures. This corresponds in the dilution refrigerator to a ^{3}He circulation rate of 30 μmole/sec at all temperatures. In the ^{3}He cryostat the same circulation rate is obtained at 0·5 K.

$$\dot{Q} = \dot{n}\left(H_{3c} - H_{3d}\right) = \dot{n}\left(\mu_{3c} - \mu_{3d} + TS_{3c} - TS_{3d}\right) =$$

The cooling power is given by: $\dot{n}T\left(S_{3c} - S_{3d}\right) = 84\ \ \dot{n}\ \ T^2\ \left[\mathrm{J/mole \cdot K^2}\right]$

Cooling power at 100 mK typically 30-1000 μW
Base temperature typically 5-30 mK (world record 1.7 mK)

Adiabatic demagnetization of paramagnetic salts

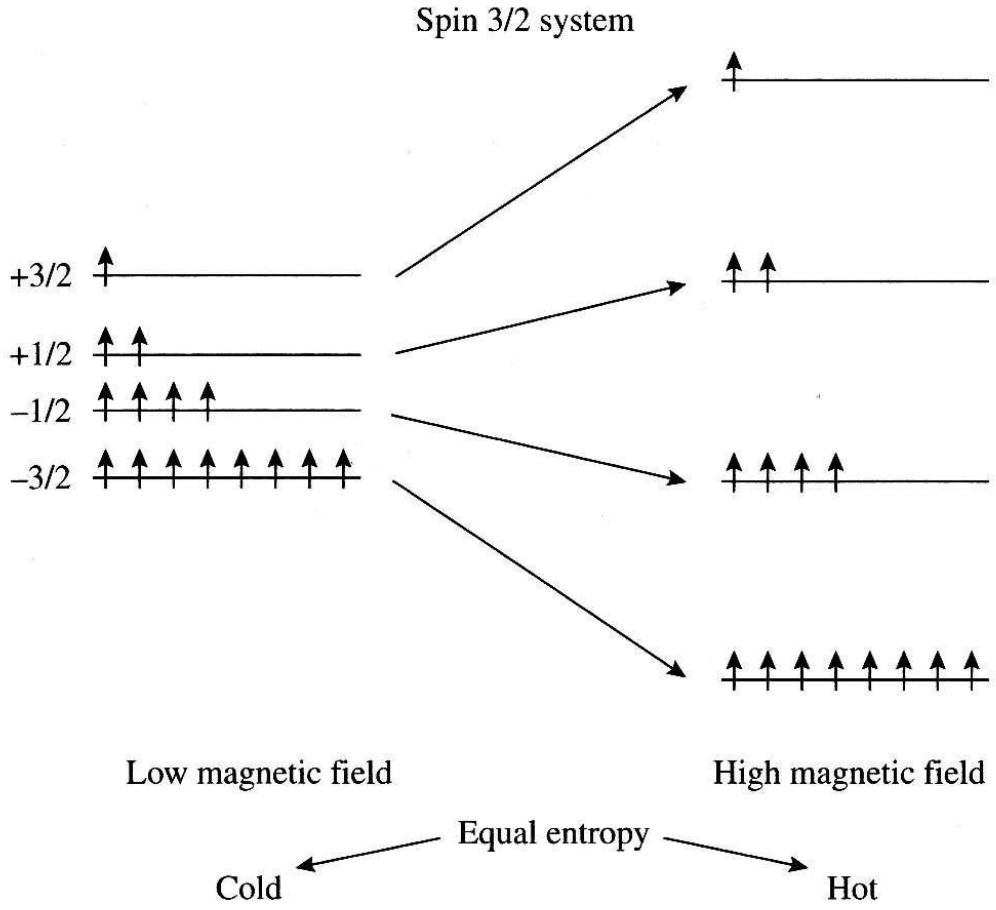

FIG. 8.4 Schematic of the spin energy levels of a paramagnet in high and low magnetic fields.

Adiabatic cooling, entropy versus temperature

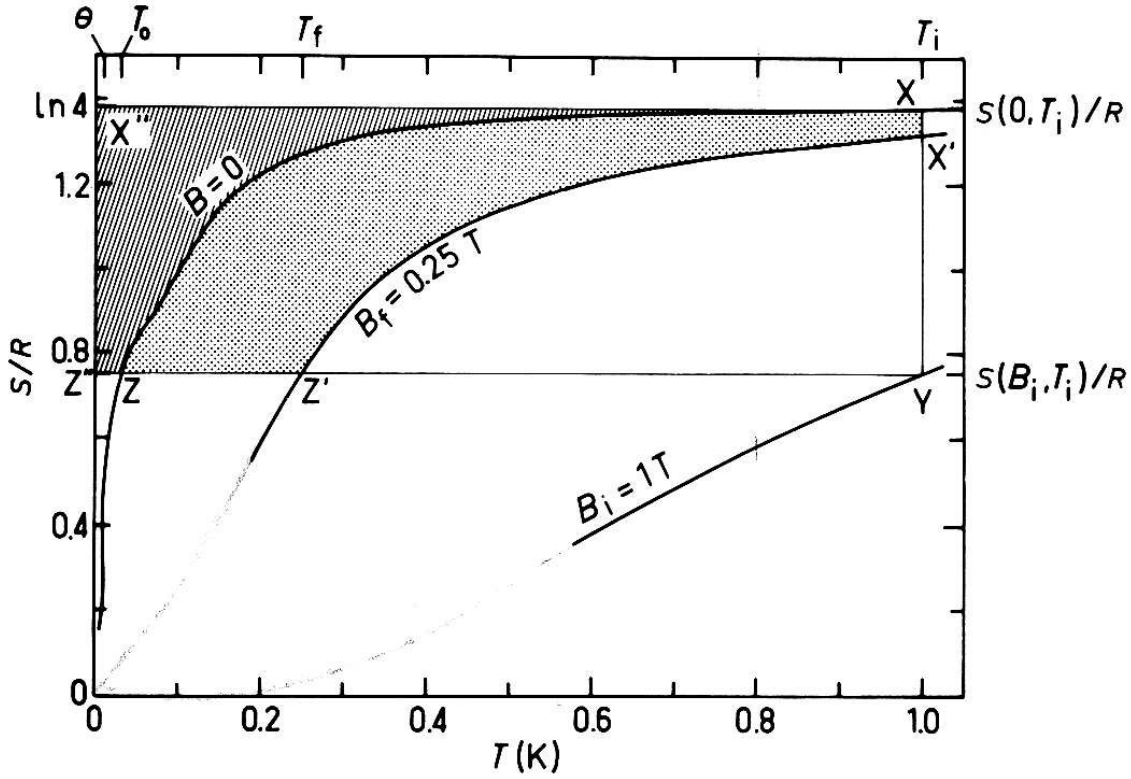

Fig. 5.1. Entropy diagram of chromic potassium alum (Bleaney, 1951; Daniels and Kurti, 1954; cf. also Section 5.3) illustrating magnetic cooling. $T_i = 1$ K, $T_f = 0{\cdot}25$ K, $T_0 = 35$ mK, $\theta = 10$ mK. For more details, see text.

What paramagnetic salts can be used

The best salt would have low ordering temperature, high spin number, and high density of spins (partly contradicting requirements)

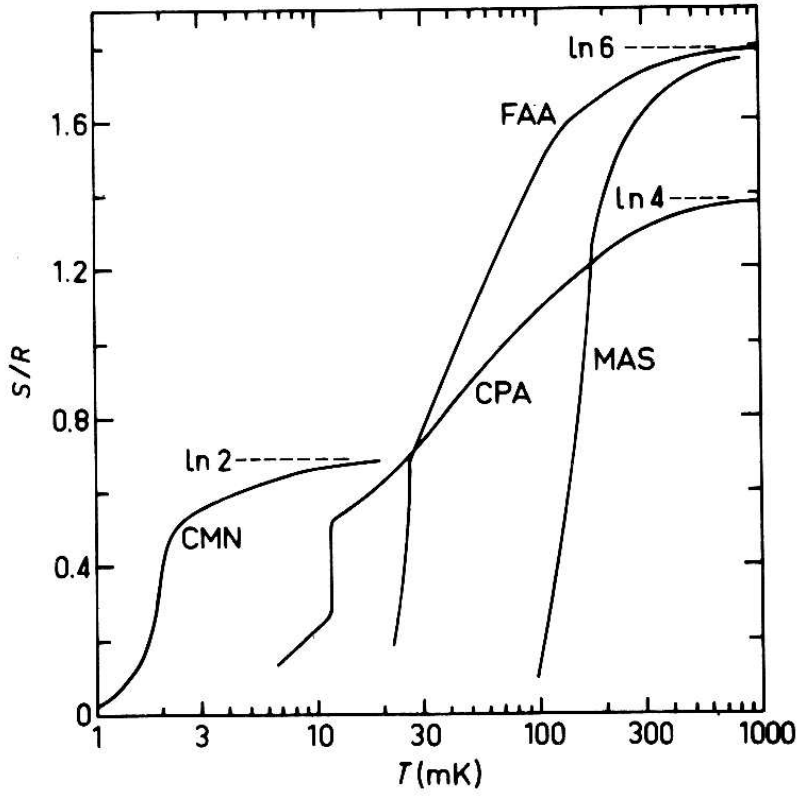

Fig. 5.4. The entropy diagrams of ferric ammonium alum (FAA), manganous ammonium sulphate (MAS), chromic potassium alum (CPA), and cerium magnesium nitrate (CMN). For a discussion and references, see text.

$$S_{max} = n R \ln(2J+1)$$

Table of paramagnetic salts

Material	m=2J+1	Bo (mT)	To (mK)	$B_{1/2}$ (1K) [T]	$B_{1/2}$ (4.2K) [T]
CMN	2	4.2	1.9	1.69	7.11
CMA	4			1.09	4.57
CPA	4	10	9	1.09	4.57
FAA	6	50	26	0.866	3.64
MAS	6	80	173	0.866	3.64

An ADR fridge

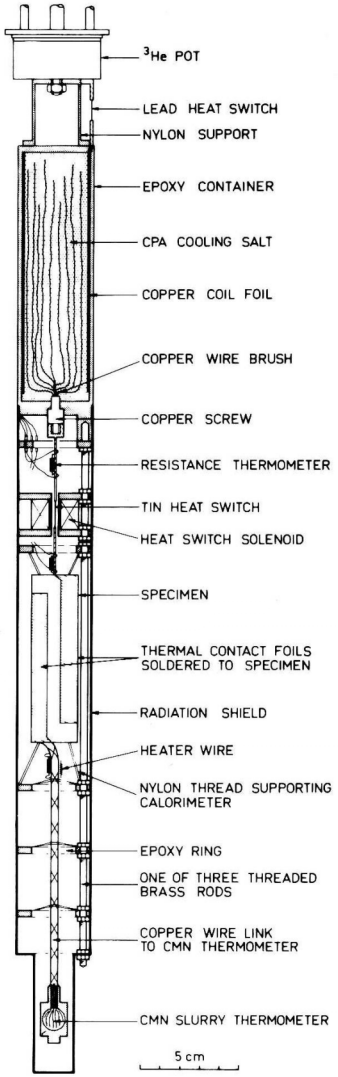

Fig. 5.8. Inner parts of the demagnetization cryostat of Krusius and Pickett (1971). The apparatus was employed for measuring nuclear heat capacities of metals between 15 mK and 0·5 K.

Adiabatic magnetization becomes modern again

Advantages: No vibrations, simple operation, lower base temp than He-3 cryostat

Drawbacks: Single shot, Low cooling power

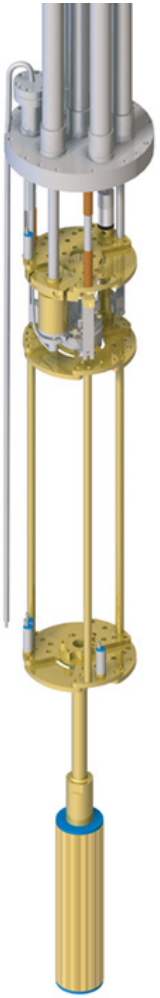

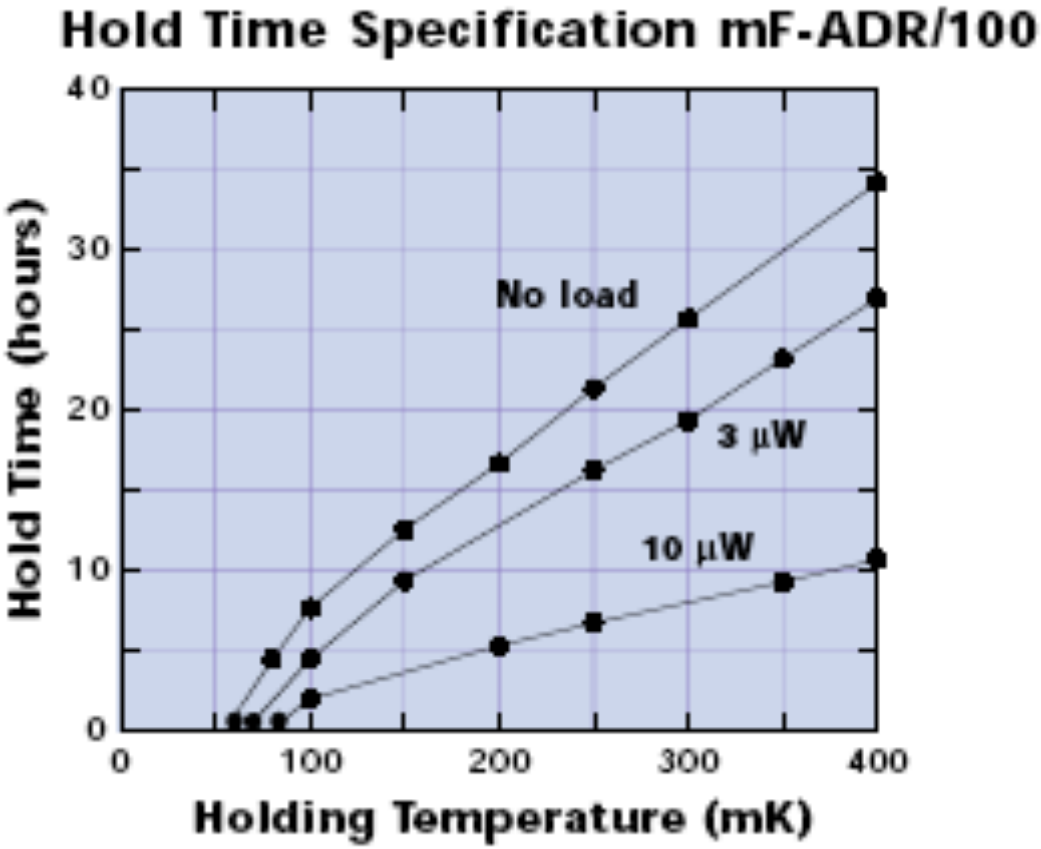

Nuclear demagnetization

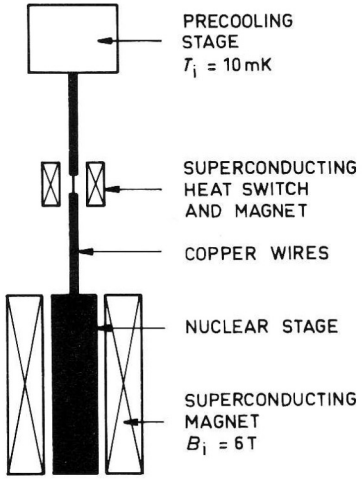

Fig. 6.1. Schematic diagram of a nuclear demagnetization cryostat. Superconducting heat switches are discussed in Section 9.5.

Starting temperature for nuclear demagnetization is much lower.

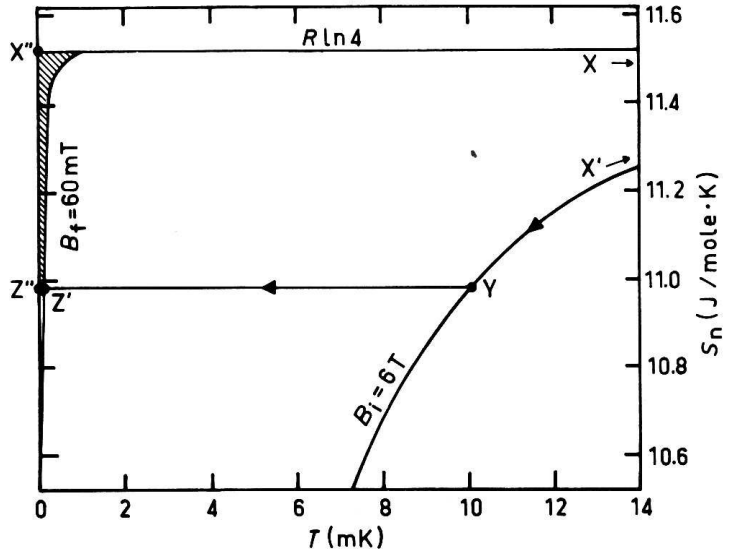

Fig. 6.3. The nuclear entropy diagram of one mole of copper (cf. Fig. 6.2). After the nuclear stage has been magnetized at about 0·5 K it is cooled along the $B_i = 6$ T curve to point Y at the starting temperature $T_i = 10$ mK. The magnetic field is then reduced adiabatically to $B_f = 60$ mT, whereby point Z′ at $T_f = 0{\cdot}1$ mK is reached. The amount of heat that must be removed from the spin system while it is magnetized to B_i and cooled to T_i is represented by the area XX′YZ″X″X (point X is at $B = 0$, $T = 0{\cdot}5$ K; point X′ at $B = 6$ T, $T = 0{\cdot}5$ K). During warm-up the nuclear system can absorb a much smaller quantity of heat, represented by the shaded area.

Multistage cooling

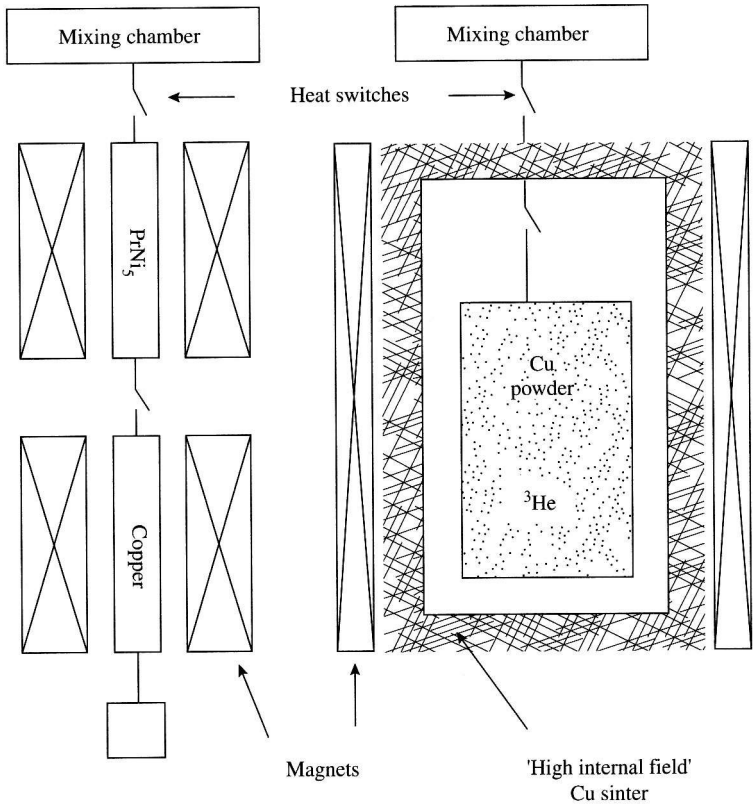

FIG. 8.6 Schematics of the two styles of multistage nuclear refrigerator. In the Julich design, left, the first stage of $PrNi_5$ 'guards' and precools the second copper stage. In the Lancaster design, right, the guard cell surrounds the final stage reducing heat leaks to a minimum. More than two stages may be present and all stages are demagnetized simultaneously. The outer stages retain their heat capacity due to spontaneous nuclear ordering phenomena or crystalline fields.

Heat Switches
Superconducting, mechanical, gas

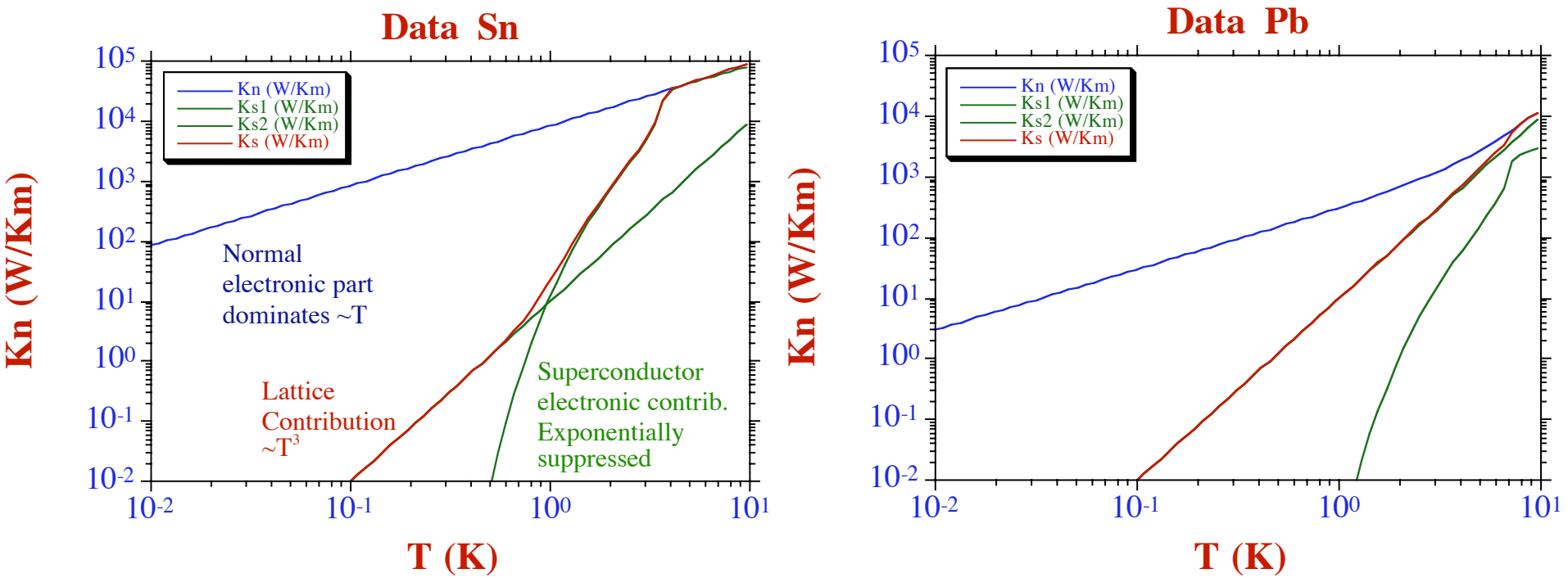

Apply a moderate magnetic field Hc to make the metal normal
and thus a much better heat conductor.

Electron Spin and Phonon temperatures can differ

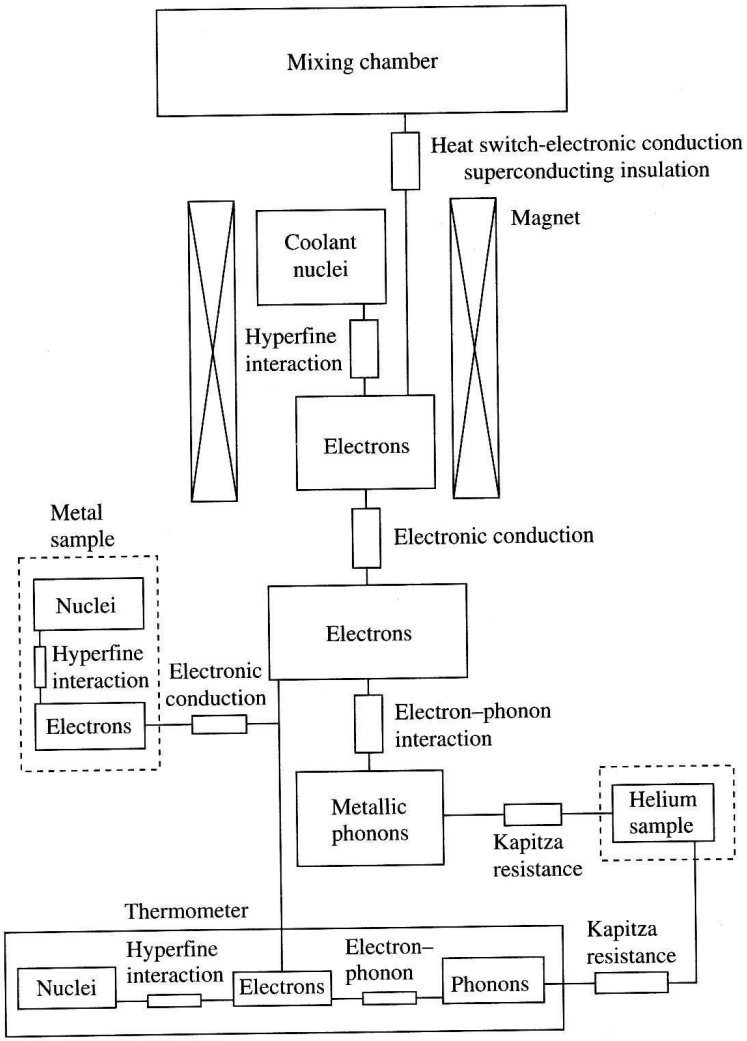

FIG. 8.5 A schematic of the various thermal reservoirs and thermal resistances involved in a nuclear cooling experiment, after Lounasmaa (1974). It is supposed that a metal specimen, a ^{3}He sample and a thermometer are to be cooled.

Pomeranchuk cooling

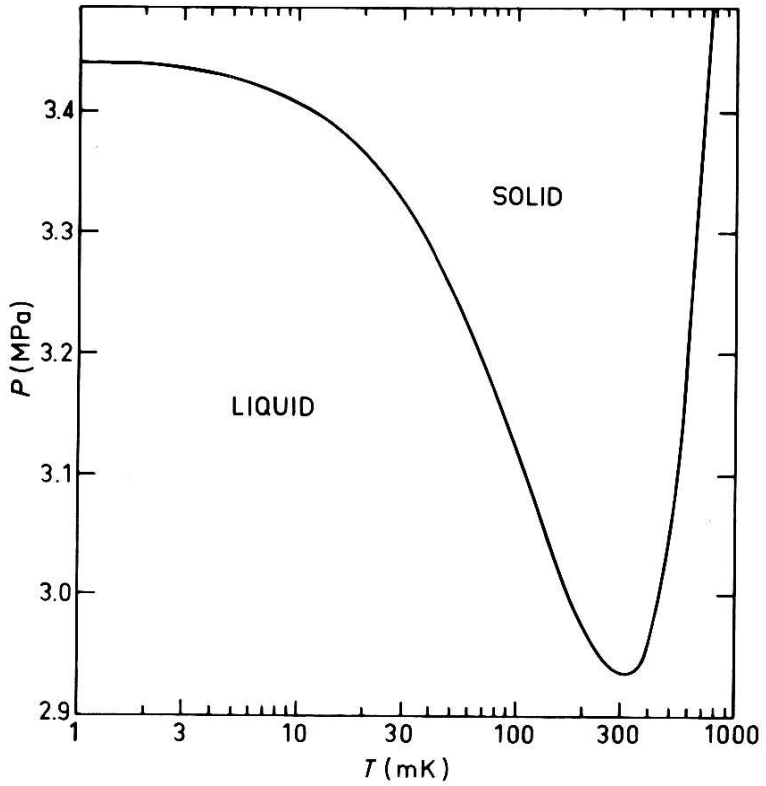

Fig. 4.1. The melting curve of ^{3}He at low temperatures.

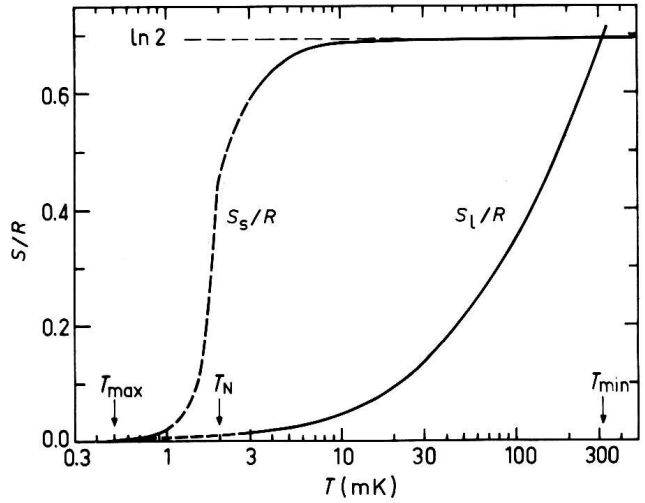

Fig. 4.2. The entropy of solid and liquid ^{3}He along the melting curve. The full nuclear spin entropy, $s_s/R = \ln(2I + 1) = \ln 2$, is marked in the figure. T_N is the antiferromagnetic transition temperature of solid ^{3}He. T_{max} and T_{min} are the temperatures at which the maximum and the minimum occur in the melting curve, respectively. At these temperatures $s_s = s_l$. This diagram is rather uncertain below 3 mK; the transitions shown in Fig. 4.15 have not been incorporated into it.

A Pomeranchuk celll

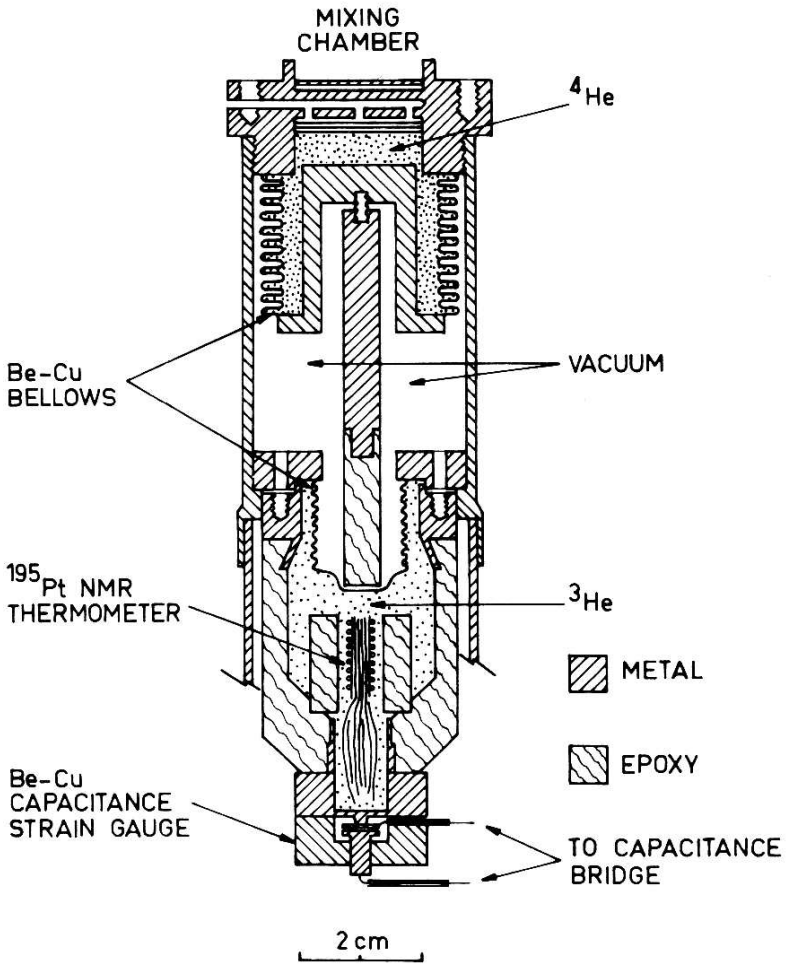

Fig. 4.11. The "hydraulic press"-type Pomeranchuk cell of Osheroff, Richardson and Lee (1972). For more details, see text.

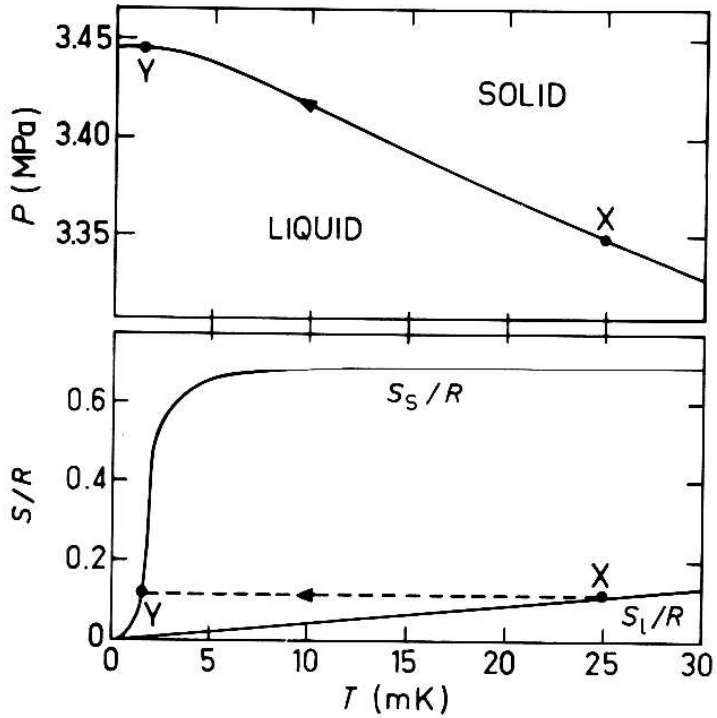

Fig. 4.3. The phase and entropy diagrams of ^{3}He demonstrating Pomeranchuk cooling.

Comparison of Cooling powers

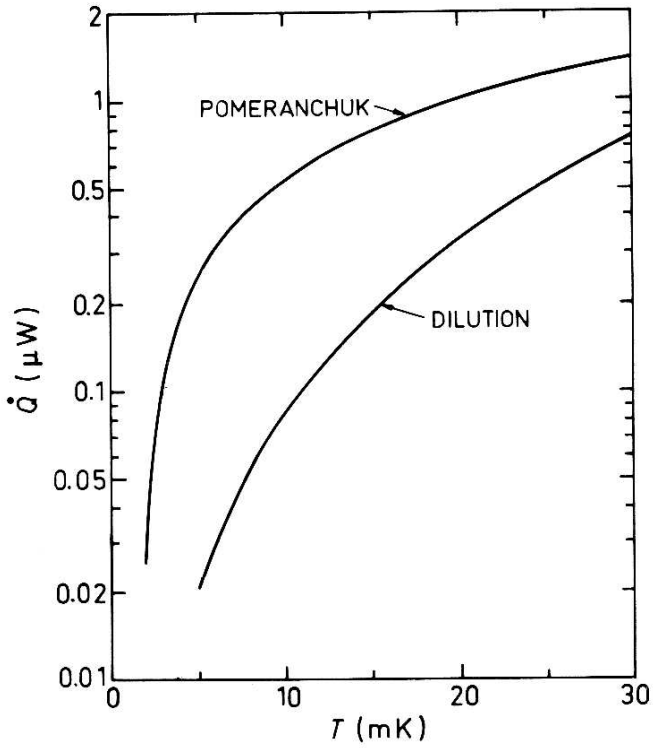

Fig. 4.5. The cooling powers of a Pomeranchuk cryostat and of a single-cycle dilution refrigerator. In the former case liquid is converted into solid at the rate 10 μmole/sec; in the latter case ^{3}He is removed from the mixing chamber at the same rate.

Thermometry below 1K

Pimary versus secondary thermometers: A primary thermometer does not need calibration.

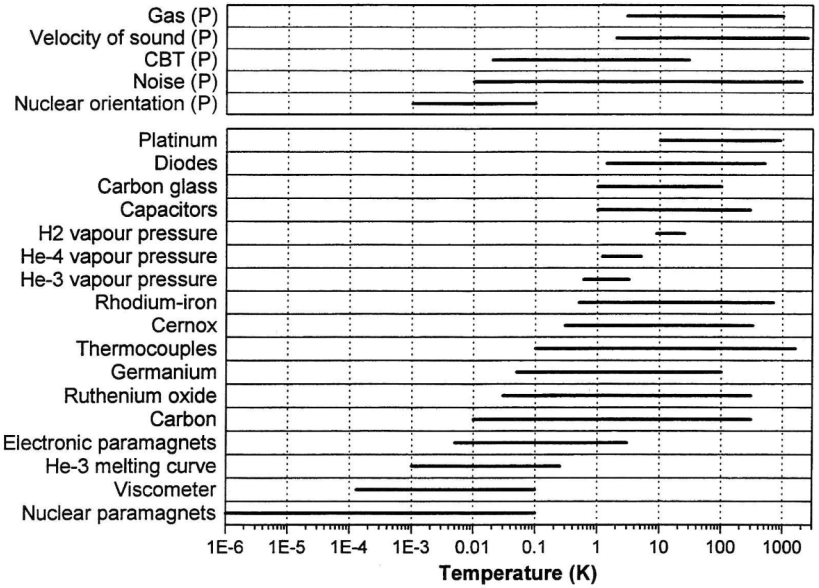

Table 1. Temperature ranges of selected cryogenic thermometers (P ↔ primary).

Primary thermometers

(Gas thermometry)
Nuclear orientation
Coulomb blockade thermometry
Noise thermometry

Nuclear orientation

The orientation of emitted gamma photons has an angular dependence at low temperature.

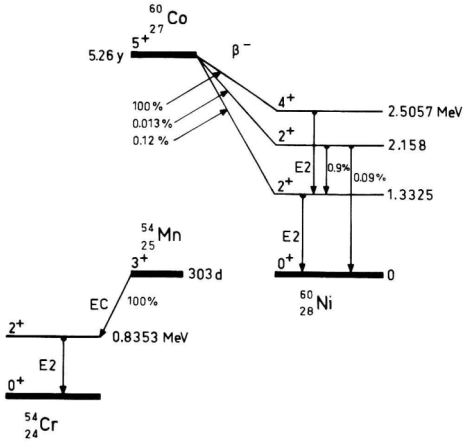

Fig. 8.2. The decay schemes of ^{60}Co and ^{54}Mn.

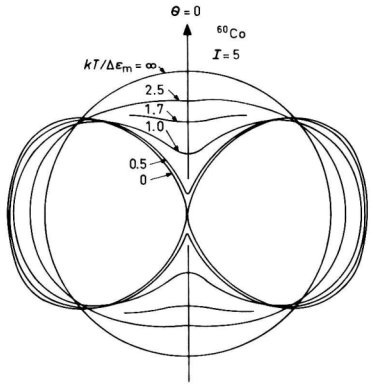

Fig. 8.3. The angular radiation pattern of ^{60}Co for several different values of $kT/\Delta\epsilon_m$.

At high T the distribution is isotropic, bot at low T some directions are preferred.

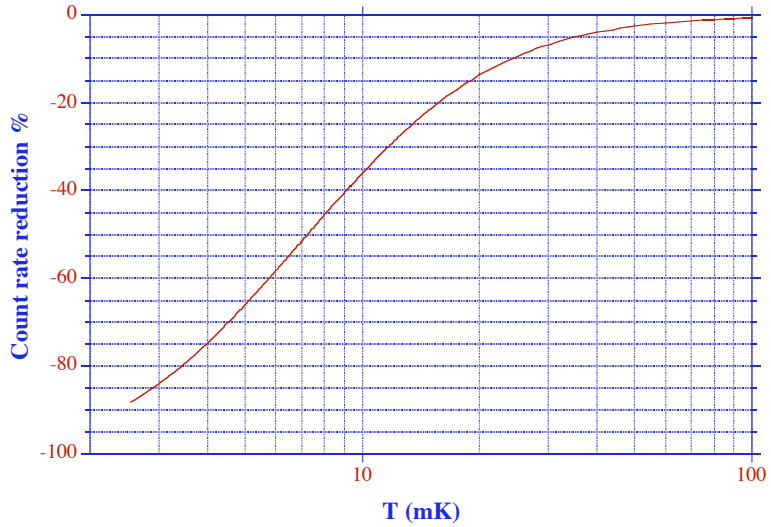

Sensitive only below 50mK

Noise thermometry

$$\overline{V}^2 = 4k_B TR\Delta f$$

The noise from a resistor depends directly on the temperature.

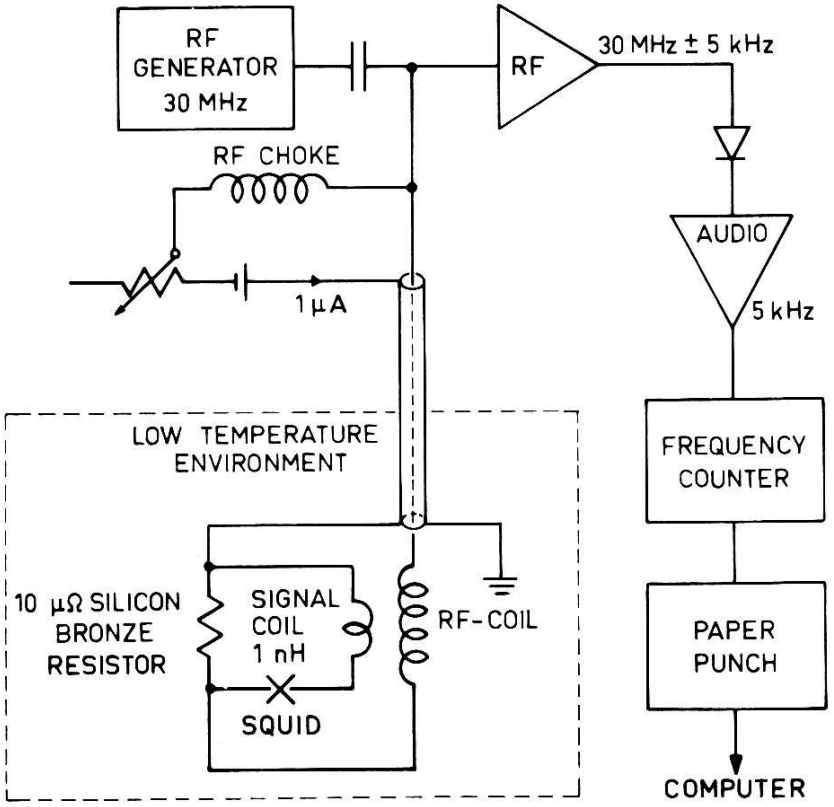

Fig. 8.13. The circuit employed by Kamper and Zimmerman (1971) and by Kamper (1973) for noise thermometry.

Coulomb blockade thermometry

The half width of the conductance dip for an array of small tunnel junctions depends only on the temperature

$$V_{\frac{1}{2}} = C\frac{Nk_BT}{e}$$

$C = 5.349...$ Caculable

$N =$ number of junctions in series

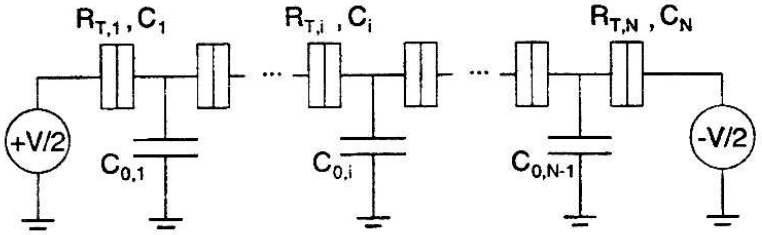

FIG. 1. Schematics of an N-junction array.

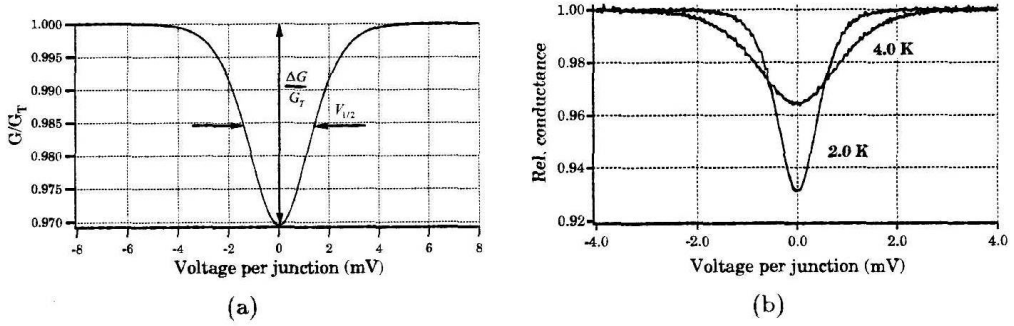

Figure 4.1.: (a) The differential conductance of a CBT sensor has an almost bell-shaped dip around zero temperature. The half-width $V_{1/2}$ depends only on the temperature and natural constants, while the depth $\Delta G/G_T$ also depends on the capacitance of the tunnel junctions. This curve was calculated from eq. 4.1. (b) Two examples of experimental curves at different temperatures. The sample was a 256×256 junction array.

Secondary thermometers

Resistive thermometers. Simplest measurement, but low excitation current needed. Often ac methods are used.

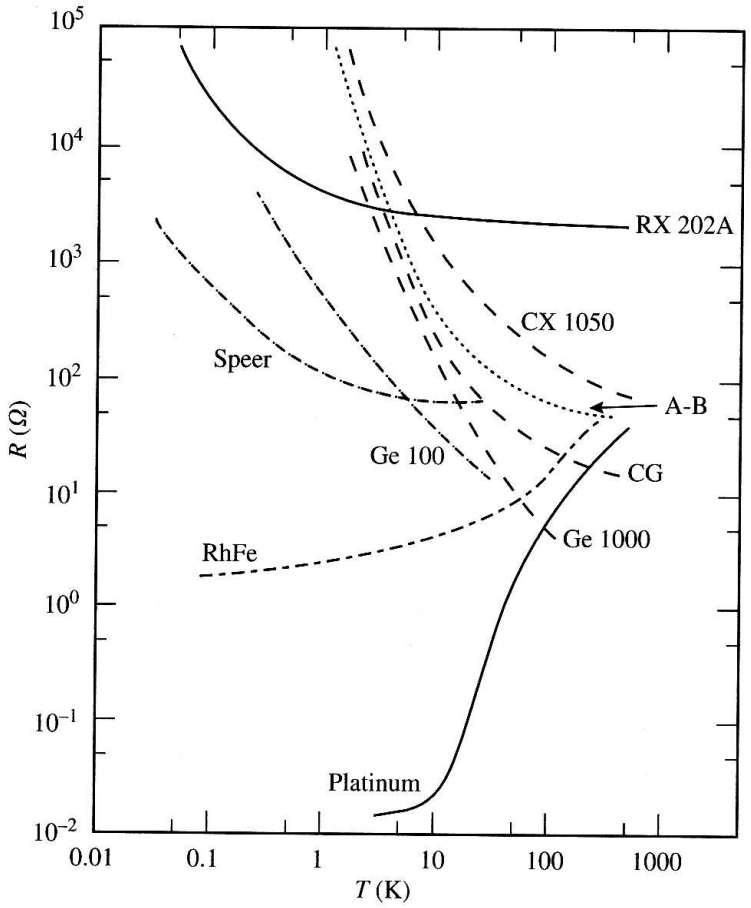

FIG. 3.7 The electrical resistance $R(T)$ of some typical thermometers. A-B denotes Allen-Bradley carbon resistor. Speer is a carbon resistor. CG is carbon-in-glass. CX 1050 is a Cernox and RX 202A is a ruthenium oxide from LakeShore. Ge 100 and Ge 1000 are Cryocal germanium thermometers.

Magnetic thermometry (CMN thermometry)

Cf. Adiabatic demagnetization

$$\chi = \frac{C}{T - \theta}, \qquad \theta = \text{the ordering temperature}$$

Signal increases with lower temperature.

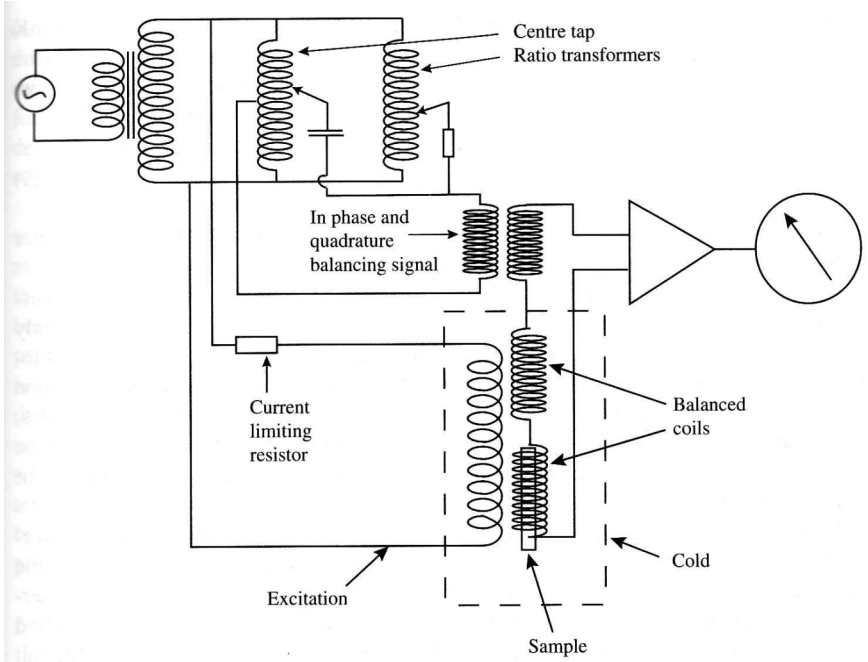

FIG. 3.13 A typical circuit for a susceptibility bridge. The amplifier and lockin may be exchanged for a SQUID.

Table 3.7 Some electronic magnetic salts used for thermometry

Salt	Abbreviation	Ordering temp. (K)
$Cr(NH_3CH_3)(SO_4)_2 \cdot 12H_2O$	CMA	0.016
$CrK(SO_4)_2 \cdot 12H_2O$	CPA	0.009
$FeNH_4(SO_4)_2 \cdot 12H_2O$	FAA	0.026
$Gd_2(SO_4)_3 \cdot 8H_2O$	GS	0.182
$Mn(NH_4)_2 \cdot (SO_4)_2 \cdot 6H_2O$	MAS	0.173
$Ce_2Mg_2(NO_3)_{12} \cdot 24H_2O$	CMN	0.002

The ordering temperature for the salt, Δ, determines the minimum temperature

He-3 melting curve thermometry

Relies on the prediction from Fermi Liquid Theory that C_V is linear with temperature

$$C_V = aT + bT^3 \ln T$$

and the Superconducting transition of tungsten, $T_{CW} \approx 12$ mK.

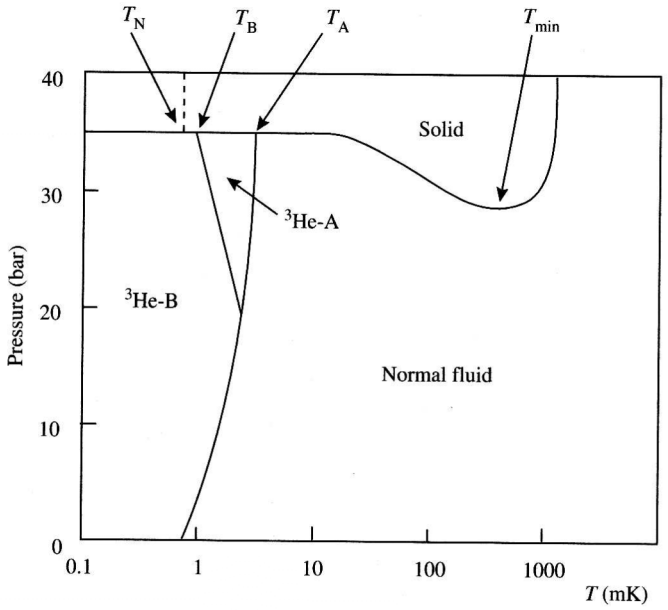

FIG. 3.14 The schematic phase diagram of ^{3}He, showing the melting curve and indicating the several fixed points.

Table 3.10 Fixed points of PLTS (2000)

	Pressure (MPa)	T_{2000} (mK)
Minimum	2.93113	315.24
T_A	3.43407	2.444
T_{AB}	3.43609	1.896
T_N	3.43934	0.902

T_N =Spin ordering temperature in the solid

Comparison of thermometers

Table 3.9 Summary of secondary temperature sensors for $T \leq 300$ K

Type	Range (K)	Sensitivity (mK)	Stability (mK)	$\Delta T/T$ (%) 2.5 T @ 4.2 K	$\Delta T/T$ (%) 2.5 T@10 K
Pt (PRT) (encaps)	>12	1	1	NA	100*
Pt (film)	>12	1–10	<100	NA	100*
RhFe (encaps)	0.5–300	1	1	11	6
RhFe (chip)	0.5–300	±10	±20	10	—
Carbon (A-B) (47, 100, 220 Ω)	0.5–100	1–10	<100	<1	<1
Carbon (Speer) (100, 220, 470 Ω)	0.5–300	1–10	<100	4–9	
Carbon-glass	1–300	1-10	5 (4.2 K) 30 (15 K)	0.5	0.2
Ge (GRT)	0.5–30	1	1–10	5–20*	4–15*
Cernox	0.3–300	±3	±20	<1	
Rox	0.02–200	10	±20	<1	
p-n junction(Si)	1–300	10	50	~100*	<50*
p-n junction(GaAlAs)	1–300	10	50	2–3*	1–2*
Capacitor ($SrTiO_3$)	0.5–60		≤500	→ 0	
Thermocouples					
Cu vs constantan	10–300	100 (>20 K)	100	see Section 3.8	
AuFe vs chromel	1–300	10 (10 K)	—	—	3

Primary thermometer	Temperature law	Performance in magnetic field	Suitable application
Gas	$pV = nRT$	Excellent	Calibrations
Nuclear orientation	$W = f(E_m/k_BT)$	Poor	Calibrations
Noise	$\langle u^2(\nu)\rangle_t = 4Rk_BT\mathrm{d}\nu$	?	Calibrations
Speed of sound	$v^2 = \gamma RT/M$	?	Calibrations
CBT	$eV_{1/2} = 5.439Nk_BT$	Excellent	Normal lab. use / calibrations

(a)

Secondary thermometers	Temperature dependence	Performance in magnetic field	Notes, (typical use)
Vapour pressure	$\exp[\Sigma a_i T^i]$	Excellent	High resolution, ITS-90
^{3}He melting curve	$\Sigma a_i T^i$	Good	High resolution and stability
Viscometer	T^{-2}	Good	No thermal contact problems
Resistors			Simple measurement
Platinum	$\Sigma a_i T^i$	Moderate	Interchangeable, ITS-90
Rhodium-iron	$\Sigma a_i T^i$	Poor	Good stability
Carbon	$\exp[\Sigma a_i (\ln T)^i]$	Poor	Cheap, high sensitivity at low T
Germanium	$\exp[\Sigma a_i (\ln T)^i]$	Poor	Stable, high sensitivity at low T
Ruthenium oxide	$\exp[\Sigma a_i (\ln T)^i]$	Moderate	Cheap, good stability
Carbon-glass	$\exp[\Sigma a_i (\ln T)^i]$	Good	High sensitivity at low T
Cernox	$\exp[f(T)]$	Good	Thin film sensor, good stability
Capacitors		Excellent	High resolution, (T-control)
Diodes		Poor	Small sensor, interchangeable
Thermoelectricity	$\Sigma a_i T^i$	Moderate	Tiny sensor, (ΔT measurements)
Electronic susceptibility	T^{-1}	Poor	Simple measurement
Nuclear susceptibility	T^{-1}	Poor	extensively used at $T < 1$ mK

(b)

Table 2. Temperature dependence, magnetic field tolerance, and some other features of the cryogenic primary thermometers in (a) and secondary thermometers in (b).